Quantitative Encapsulation and Retention of ^{227}Th and Decay Daughters in Core–Shell Lanthanum Phosphate Nanoparticles

Quantitative Encapsulation and Retention of ^{227}Th and Decay Daughters in Core–Shell Lanthanum Phosphate Nanoparticles

M. Toro-González[1,2](✉), A. N. Dame[2], C. M. Foster[3], L. J. Millet[4], J. D. Woodward[2], J. V. Rojas[1], S. Mirzadeh[2], S. M. Davern[2](✉)

[1] Department of Mechanical and Nuclear Engineering, Virginia Commonwealth University, Richmond 23284, USA
[2] Isotope and Fuel Cycle Technology Division, Oak Ridge National Laboratory, Oak Ridge 37830, USA
[3] Biosciences Division, Oak Ridge National Laboratory, Oak Ridge 37830, USA
[4] Biosciences Division, Oak Ridge National Laboratory, Oak Ridge 37830, USA; Joint Research Activity, The Bredesen Center, University of Tennessee, Knoxville 37996, USA

ORCID: 0000-0003-3320-423X (M. Toro-González), 0000-0002-9577-5006 (A. N. Dame), 0000-0001-6443-2505 (L. J. Millet), 0000-0002-2268-4613 (J. V. Rojas), 0000-0002-1774-7958 (S. Mirzadeh), 0000-0003-2755-8912 (S. M. Davern)

Address correspondence to M. Toro-González (torogonzalezm@vcu.edu, torogonzalmt@ornl.gov) and S. M. Davern (davernsm@ornl.gov)

Abstract
Targeted alpha therapy (TAT) offers a great promise for treating recalcitrant tumors and micrometastatic cancers. One drawback of TAT is the potential damage to normal tissues and organs due to the relocation of decay daughters from the treatment site. The present study evaluates La(^{227}Th)PO$_4$ core (C) and core +2 shells (C2S) nanoparticles (NPs) as delivery platform of ^{227}Th to minimize systemic distribution of decay daughters, ^{223}Ra and ^{211}Pb. *In vitro* retention of decay daughters within La(^{227}Th)PO$_4$ C NPs was influenced by the concentration of reagents used during synthesis, in which the leakage of ^{223}Ra was between $0.4 \pm 0.2\%$ and $20.3 \pm 1.1\%$ in deionized water. Deposition of two nonradioactive LaPO$_4$ shells onto La(^{227}Th)PO$_4$ C NPs increased the retention of decay daughters to >99.75%. The toxicity of the nonradioactive LaPO$_4$ C and C2S NP delivery platforms was examined in a mammalian breast cancer cell line, BT-474. No significant decrease in cell viability was observed for a monolayer of BT-474 cells for NP concentrations below 233.9 μg/mL, however cell viability decreased below 60% when BT-474 spheroids were incubated with either LaPO$_4$ C or C2S NPs at concentrations exceeding 29.2 μg/mL. La(^{227}Th)PO$_4$ C2S NPs exhibit a high encapsulation and *in vitro* retention of radionuclides with limited contribution to cellular cytotoxicity for targeted alpha therapy applications.

Keywords
Thorium-227, radium-223, lanthanum phosphate, nanoparticles, targeted alpha therapy

1 Introduction

Lanthanide-based compounds have been proposed as platforms to encapsulate and immobilize radionuclides for nuclear medicine and nuclear waste management. Specifically, naturally occurring monazite and xenotime lanthanide phosphate compounds can contain high levels of Th, U, decay daughters, and fission products without experiencing radiation-induced amorphization.[1–3] This transition from crystalline to amorphous, induced primarily by α-decay, is characterized by a collapse of the crystal structure and a loss of periodicity of the atoms and relationships within the crystal structure.[4] The resistance to radiation damage of synthetic monazite and xenotime lanthanide phosphate compounds has been demonstrated experimentally and by simulations.[5–9] Experimentally, synthetic lanthanide phosphate compounds have been subjected to either self-irradiation with short-lived minor actinides or ion-beam irradiation.[2,4,7,10,11] Results showed that synthetic lanthanide phosphate compounds remained largely crystalline because the crystal structure recovers from the damage caused by the recoil nucleus and the α-particle during an α-decay event.[4] Conversely, simulations demonstrated that lanthanide phosphate compounds with monazite structure are more resistant to radiation damage compared with those with xenotime structure.[6] Additionally, the high chemical durability, low solubility, and mechanical stability of lanthanide phosphate compounds make them promising platforms for encapsulation and immobilization of α-emitting radionuclides.[1,8,12]

Woodward et al. proposed using lanthanum phosphate nanoparticles (NPs) as an ^{225}Ac delivery platform for targeted alpha therapy (TAT) to minimize the relocation of decay daughters from the target site.[13] *In vitro* retention of decay daughters ^{221}Fr and ^{213}Bi was ~40%, whereas functionalized La(^{225}Ac)PO$_4$ NPs retained ~87% of ^{213}Bi *in vivo*, 120 h post-injection.[13] In a subsequent study, the *in vitro* retention of ^{221}Fr was enhanced to 90.9 ± 0.9% by developing a core–shell structure composed of a La$_{0.25}$Gd$_{0.75}$PO$_4$ core, four GdPO$_4$ shells, and a gold layer.[14] *In vivo* studies showed that 84 ± 3% of the injected dose from ^{213}Bi was retained in lung tissue and less than 3% migrated to the kidneys 24 h post-injection when using functionalized core–shell NPs.[15] These results are of utmost importance because renal toxicity caused by the relocation of ^{213}Bi is one of the limiting factors of using ^{225}Ac for patient treatment.[14] Core–shell La(^{223}Ra)PO$_4$ structures were also studied for the encapsulation of ^{223}Ra and the retention of its decay daughters, where a quantitative retention of both ^{223}Ra and ^{211}Pb was obtained *in vitro* using La(^{223}Ra)PO$_4$ core +2 shells NPs.[16] The promising results obtained with La(^{223}Ra)PO$_4$ core +2 shells NPs could contribute to the application of radium radionuclides for cancer treatment beyond bone diseases after modification of their surface for facile attachment of the NP-construct to targeting vectors including aptamers, peptides, and antibodies. Overall, the partial encapsulation and retention of α-emitting radionuclides, and the multimodal molecular imaging capabilities of lanthanide phosphate NPs, make them a unique platform for theranostic applications.[17–21]

The clinical efficacy of Xofigo® (^{223}RaCl$_2$) has encouraged the development of radiopharmaceuticals based on α-emitting radionuclides.[22] Thorium-227 (T$_{1/2}$ = 18.7 d) is an α-emitting radionuclide in the ^{227}Ac decay chain that has gained significant attention for its potential use in TAT. Similarly to ^{223}Ra, ^{227}Th can be produced in large quantities from the ß-decay of ^{227}Ac, which in turn is

produced via neutron irradiation of a ^{226}Ra target in a nuclear reactor.[23] In contrast to ^{223}Ra, ^{227}Th can form stable complexes with chelating ligands such as 1,4,7,10-Tetraazacyclododecane-1,4,7,10-tetraacetic acid (DOTA) and 1-methyl-3-hydroxy-pyridin-2-one (Me-3,2-HOPO) for the synthesis of targeted thorium conjugates.[24–32] Organic and inorganic NPs have also been proposed as delivery platforms that encapsulate therapeutic α-emitting radionuclides such as $^{223/224/225}$Ra, ^{225}Ac, and ^{227}Th. Liposomes and polymersomes are the main organic NPs that have been studied for TAT applications,[33–42] whereas inorganic NPs include compounds such as lanthanide phosphate,[13–16] gadolinium vanadate,[43,44] zeolites,[45,46] iron oxide,[47,48] hydroxyapatite,[49–51] gold,[52] calcium carbonate,[53,54] barium sulfate,[55] titanium dioxide,[56] and polyoxopalladate.[57] Motivated by the promising application of ^{227}Th and nanomaterials in TAT, La(^{227}Th)PO$_4$ core (C) and core +2 shells (C2S) NPs were evaluated as delivery platforms of ^{227}Th to minimize the relocation of decay daughters from the target site. The selection of La(^{227}Th)PO$_4$ C and C2S NPs is based on the promising results obtained with both ^{225}Ac and ^{223}Ra.[14,16] Partial encapsulation and retention of ^{227}Th and decay daughters was obtained *in vitro* using La(^{227}Th)PO$_4$ C NPs, whereas >99.75% of the initial activity of ^{227}Th, ^{223}Ra, and ^{211}Pb was retained in La(^{227}Th)PO$_4$ C2S NPs. These results combined with the results obtained with ^{225}Ac[13–15] and $^{223/225}$Ra[16] demonstrate the remarkable ability of lanthanide phosphate NPs to act as delivery platforms for α-emitting radionuclides. The cytotoxicity of LaPO$_4$ C and C2S NPs on RAW 264.7 murine macrophage and BT-474 human breast cancer cells were assessed based on their potential application in biological systems. RAW 264.7 cells were selected because they represent an appropriate model of macrophages that are capable of performing both phagocytosis and pinocytosis.[58] Overall, core–shell LaPO$_4$ NPs are promising radionuclide delivery platforms for theranostic applications that have inherently low cytotoxicity, exhibit a high retention of ^{227}Th and decay daughters, and can potentially incorporate multimodal imaging functionalities.

2   Experimental section

2.1   Reagents and Materials

LaCl$_3$·7H$_2$O (99.9%) and Na$_5$P$_3$O$_{10}$ (>98%) were purchased from Sigma Aldrich (St. Louis, MO) and used without further purification. A Milli-Q® water purification system was used to obtain deionized water (18 MΩ·cm). Spectra/Por® biotech regenerated cellulose membrane with an 8–10 kDa molecular weight cutoff (Repligen Corporation, Waltham, MA) was used for NP purification. Thorium-227 was obtained from ^{227}Ac ($T_{1/2}$ = 21.7 years) generated via thermal neutron irradiation of a ^{226}Ra target. Recovery of carrier-free ^{227}Th was achieved using an anion exchange resin (BIO-RAD AG® MP1-M 100-200 mesh). First, 0.1 M HNO$_3$ with ^{227}Th in equilibrium with decay daughters was loaded on a 0.3 mL column of MP1-M resin. Radium-223 and decay daughters were eluted from the column after washing with 8 column volumes of 8 M HNO$_3$, subsequently 8 column volumes of 0.1 M HNO$_3$ were used to obtain carrier-free ^{227}Th. Radiochemical synthesis of La(^{227}Th)PO$_4$ C and C2S NPs was carried out using carrier-free ^{227}Th(NO$_3$)$_4$.

2.2   Synthesis of La(^{227}Th)PO$_4$ C and C2S NPs

The synthesis of La(^{227}Th)PO$_4$ C and C2S NPs was completed in aqueous media by precipitation of La^{3+} and [PO$_4$]$^{3-}$ from LaCl$_3$·7H$_2$O and Na$_5$P$_3$O$_{10}$.[59,60] Three synthesis procedures were followed to

prepare La(^{227}Th)PO$_4$ C and C2S NPs by varying either the volume or concentration of reagents (Table 1), while following the same synthetic steps. Briefly, a 1:1 volume ratio of LaCl$_3$:Na$_5$P$_3$O$_{10}$ was used for the synthesis of La(^{227}Th)PO$_4$ C NPs at two reagent concentrations, 0.1 M (procedure A) and 0.01 M (procedure C). In procedure B, La(^{227}Th)PO$_4$ C NPs were prepared using a 1:2 volume ratio of LaCl$_3$:Na$_5$P$_3$O$_{10}$ with both reagents at 0.1 M. Initially, a 0.1 M HNO$_3$ solution containing 12–49 µCi of ^{227}Th was evaporated to dryness inside a 3 mL Pyrex V-vial using an infrared heat lamp and a hot plate. The LaCl$_3$ solution was added to the vial and stirred for 10–15 min. Then, the Na$_5$P$_3$O$_{10}$ solution was added drop-by-drop under constant stirring, and the mixture was heated at 90°C for 3 h using a Reacti-Therm™ heating and stirring module. After synthesis, the La(^{227}Th)PO$_4$ C NP suspension appeared turbid and was dialyzed overnight against deionized water and then divided into two equal parts: one for radionuclide retention studies and the other for core–shell synthesis. The deposition of the first nonradioactive LaPO$_4$ shell was completed by mixing a solution containing a 1:2 volume ratio of LaCl$_3$:Na$_5$P$_3$O$_{10}$ with the dialyzed La(^{227}Th)PO$_4$ C NP suspension (Table 1) and heating this mixture at 90°C for 3 h using a Reacti-Therm™ heating and stirring module. The deposition of the second shell was completed by adding a solution containing a 1:2 volume ratio of LaCl$_3$:Na$_5$P$_3$O$_{10}$ (Table 1) into the ongoing shell reaction, while heating for an additional 3 h. The turbid La(^{227}Th)PO$_4$ C2S NP suspension was dialyzed overnight to remove unreacted radionuclides, and then the dialysate was replaced with fresh deionized water to assess the retention of radionuclides over time. For characterization purposes, nonradioactive core–shell LaPO$_4$ NPs were synthesized following the same concentrations, volume ratios, and synthetic steps described for La(^{227}Th)PO$_4$ C and C2S NPs.

Table 1 Volume and concentration of reagents used for the synthesis of La(^{227}Th)PO$_4$ C and C2S NPs.

Procedure	Volume and concentration of reagents							
	Core				Shells			
	LaCl$_3$		Na$_5$P$_3$O$_{10}$		LaCl$_3$		Na$_5$P$_3$O$_{10}$	
	Vol. (µL)	Conc. (M)	Vol. (µL)	Conc. (M)	Vol. (µL)	Conc. (M)	Vol. (µL)	Conc. (M)
A	500	0.1	500	0.1	250	0.1	500	0.1
B	500	0.1	1,000	0.1	250	0.1	500	0.1
C	500	0.01	500	0.01	250	0.01	500	0.01

2.3 Characterization of LaPO$_4$ C and C2S NPs

LaPO$_4$ C and C2S NPs suspensions were precipitated by centrifugation, dried at 80°C for 8 h in a muffle furnace, and then ground using a mortar and pestle. Powder X-ray diffraction was performed using a PANanalytical X'Pert Pro MPD X-ray diffractometer operated at 45 kV and 40 mA with a Cu anode (Cu k$_\alpha$, λ = 1.504 Å). The NP morphology was assessed using transmission electron microscopy in a FEI Titan (300 kV) and a Zeiss Libra (120 kV). LaPO$_4$ C and C2S NP suspensions were diluted 100 times in deionized water and then drop-casted onto a 300 mesh formvar/carbon copper grid. The

particle size distribution and zeta potential of LaPO$_4$ C and C2S NP suspensions diluted either 100 (procedures A and B) or 10 (procedure C) times in phosphate buffered saline (1X, pH 7.2) were characterized by dynamic light scattering and phase analysis light scattering using a ZetaPALS (Brookhaven Instruments Corporation, NY). The stability of LaPO$_4$ C NPs (procedure A) was assessed based on the concentration of La cations in the dialysate after dialyzing the NP suspensions against deionized water at different hydrogen ion concentrations. Deionized water (pH 5.7) was used as a control for stability studies since the evaluation of encapsulation and retention of radionuclides was carried out with this solvent. LaPO$_4$ C NPs were also subjected to both acidic (pH 2.4 and 3.5) and alkaline (pH 8.8 and 10) conditions by adjusting the dialysate's pH with 1 M HCl and 1 M NaOH. Aliquots were taken periodically (4, 24, 48, and 72 h) from the dialysate and the concentration of La was determined by inductively coupled plasma–optical emission spectroscopy using an Agilent 5110. An inductively coupled plasma standard containing 1,000 ppm of La was serially diluted from 100 to 0.1 ppm to build a calibration curve. The particle size distribution and zeta potential of LaPO$_4$ NP suspensions dialyzed at different hydrogen ion concentrations were characterized as prepared and without further dilution using a NanoPlus HD (Micromeritics®). Chemical yields of LaPO$_4$ C NPs were also determined by measuring the La cation concentration after dialysis of the NP suspension against deionized water. Elemental composition analysis by X-ray photoelectron spectroscopy was carried out using a ThermoFisher Escalab 250 with a monochromated aluminum X-ray source. Sample preparation consisted of drop-casting LaPO$_4$ C NP suspensions before and after dialysis onto a silicon wafer and allowed to dry. Software CasaXPS 2.23.22 was used for spectra analysis.

2.4   Radionuclide encapsulation in La(^{227}Th)PO$_4$ C and C2S NPs

Radionuclide encapsulation was evaluated *in vitro* by dialyzing both La(^{227}Th)PO$_4$ C and C2S NPs against deionized water as reported previously.[13,14,16,43,44] The activity of ^{227}Th, ^{223}Ra, and ^{211}Pb was determined by γ-ray spectroscopy using a high-purity germanium detector (Ortec, Oak Ridge, TN) with a crystal active volume ~100 cm^3 and a Be window that was coupled to a PC-based multichannel analyzer (Canberra Industries, Meriden, CT). The γ-ray energies and intensities used to determine the activity of each radionuclide were ^{227}Th (235.9 keV, 12.9%), ^{223}Ra (269.5 keV, 13.9%), and ^{211}Pb (404.8 keV, 3.8%).[61] Energy and efficiency calibrations were determined by γ-ray sources traceable to the National Institute of Standards and Technology. For La(^{227}Th)PO$_4$ C and C2S NPs prepared following procedures B and C, the leakage and error bars were calculated from a single experiment considering the error propagation from the uncertainties associated to pipetting, detector efficiency, and activity measurement. The leakage of ^{211}Pb was corrected to account only for the fraction of activity leaking from La(^{227}Th)PO$_4$ C and C2S NPs rather than that originating from ^{223}Ra in the dialysate. Radionuclide leakage was calculated from the ratio between the activity in the dialysate aliquot and the activity of the NP suspension within the dialysis membrane, after adjusting for volume loss due to the aliquots withdrawn and radioactive decay. The radiochemical yield of ^{227}Th was calculated based on the initial activity, the activity lost during synthesis in the Pyrex V-vial and pipette tips, and the total activity lost during dialysis.

2.5 Cytotoxicity of LaPO$_4$ C and C2S NPs

RAW 264.7 murine macrophage and BT-474 human breast cancer cell lines were obtained from the American Type Culture Collection (ATCC®, Manassas, VA). Cells were seeded in a 75 cm^2 cell culture flask (Corning®) and cultured at 37°C in humidified air containing 5% CO$_2$. A 1:1 mixture of Dulbecco's Modified Eagle's Medium and Ham's F12 medium supplemented with 10% fetal calf serum, 2 mM L-glutamine, 100 I.U./mL penicillin, and 100 μg/μL streptomycin, was used to culture both cell lines (DMEM/F12 complete medium). RAW-264.7 cells were passaged by scraping, while trypsinization was used for BT-474 cells. Approximately 1×10^5 RAW 264.7 cells per well were seeded in a flat-bottom tissue culture–treated 96-well plate (Corning® Costar®) and incubated for 24 h at 37°C in humidified air containing 5% CO$_2$. Similarly, 3×10^3 BT-474 cells per well were seeded in either a flat-bottom tissue culture treated 96-well plate (Corning® Costar®) or a U-bottom cell culture 96-well microplate (Greiner Bio-One, Monroe, NC), followed by 72 h of incubation at 37°C in humidified air containing 5% CO$_2$. BT-474 spheroids were formed in non-adherent U-bottom microplates, while tissue culture treated flat-bottom plates were used to grow monolayers. Both configurations were used to assess the toxicity of nonradioactive LaPO$_4$ C and C2S NPs.

Cytotoxicity assessment of nonradioactive LaPO$_4$ C and C2S NPs was performed using 3 (4,5-dimethylthiazol-2-yl)-2,5-diphenyltetrazolium bromide (MTT) and CellTiter-Glo® 3D (Promega) assays. A serial dilution of LaPO$_4$ C and C2S NPs in DMEM/F12 complete medium from 1,871 μg/mL to 29.2 μg/mL was added to each plate in triplicate. The proposed concentrations encompass a broad range, which were chosen based on previous research performed with LaPO$_4$:Tb nanorods.[62] This information will serve as a baseline reference for further *in vitro* and *in vivo* assessment of radioactive LaPO$_4$ NPs. After 24 h of incubation, the MTT assay was performed, on the monolayer cultures, as reported by Mosmann et al.,[63] and the absorbance was measured 3 h after the addition of isopropanol, using a Cytation 1 cell imaging reader (BioTek Instruments Inc., Winooski, VT). The BT-474 spheroids were incubated for 24 h in the presence of the NPs and then assayed using the CellTiter-Glo® 3D following the reported protocol.[64] The percentage of cell viability was calculated from the ratio of either the absorbance or luminescence of treated cells with respect to those untreated.

3 Results and Discussion

3.1 Synthesis of LaPO$_4$ C and C2S NPs

The reagent concentrations and volume ratios proposed in procedure A were selected based on the results obtained with La(^{223}Ra)PO$_4$ core-shell NPs,[16] while the magnitudes used in procedure B are based on the results reported for Ln(^{225}Ac)PO$_4$ core-shell NPs.[14] It is expected that increasing the LaCl$_3$:Na$_5$P$_3$O$_{10}$ volume ratio from 1:1 (procedure A) to 1:2 (procedure B) will result in La(^{227}Th)PO$_4$ C NPs having a narrower size distribution. The reason for decreasing the reagent concentration from 0.1 M (procedures A and B) to 0.01 M (procedure C) during the synthesis of LaPO$_4$ C and C2S NPs was to increase the ^{227}Th/La ratio by one order of magnitude. To a certain extent, this experiment will simulate the capacity of LaPO$_4$ core-shell NPs to encapsulate a higher fraction of radionuclides and thus higher specific activities. Overall, the pH of the LaCl$_3$-Na$_5$P$_3$O$_{10}$ mixture was higher than that of the LaPO$_4$ C NP suspension for the different synthesis procedures (Table S1 in the electronic supporting

information; ESI). Dialyzing the NP suspension against deionized water or a buffer can aid in adjusting the suspension's pH to a specific value (Table S1 in the ESI). Modifying the $LaCl_3$:$Na_5P_3O_{10}$ ratio did not influence the particle formation, where the chemical yield of $LaPO_4$ C NPs was $96.6 \pm 0.2\%$ and $94.7 \pm 0.4\%$ for samples prepared following procedures A and B, respectively. X-ray photoelectron analysis showed that the elemental composition of $LaPO_4$ C NPs includes mainly La, P, and O (Fig. S1 in the ESI). Among additional elements observed in the spectra, there was a significant difference in the fraction of sodium before and after dialysis of $LaPO_4$ C NPs. These sodium cations, which originate from the reagents used for synthesis, segregate, or accumulate on the surface of $LaPO_4$ C NPs (Fig. S1a in the ESI). Dialysis of $LaPO_4$ C NP suspensions successfully removes all unreacted sodium from the NPs (Fig. S1b in the ESI).

3.2   Crystal structure and morphology of $LaPO_4$ C and C2S NPs

A hexagonal crystal system with space group $P6_222$ (powder diffraction file: 01-075-1881) was obtained for $LaPO_4$ C and C2S NPs synthesized as described for Procedure A (Fig. 1). An increase in the crystallite size from 4.1 ± 0.5 nm to 5.6 ± 0.2 nm is consistent with an epitaxial growth after the deposition of two $LaPO_4$ shells onto the $LaPO_4$ C NPs.[59] As shown in Fig. S2 in the ESI, $LaPO_4$ C NPs synthesized using procedure B are characterized by a hexagonal crystal system and a crystallite size of 4.0 ± 1.1 nm. It is expected that the deposition of two $LaPO_4$ shells onto $LaPO_4$ C NPs prepared following procedure B will yield a similar increase in crystallite size as was obtained using procedure A.
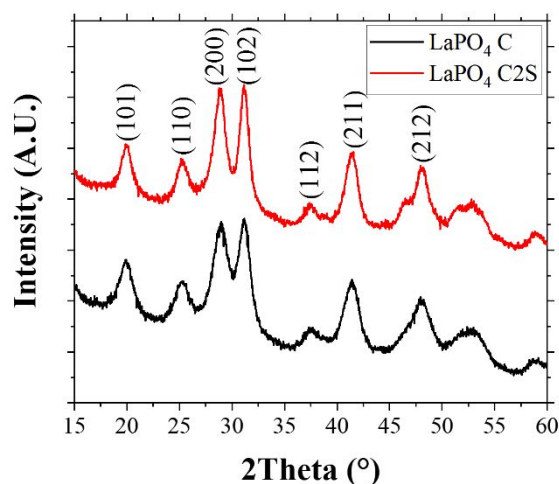
Fig. 1 Increase in crystallite size after deposition of two $LaPO_4$ shells onto $LaPO_4$ C NPs. Diffraction patterns of $LaPO_4$ C and C2S NPs synthesized following procedure A.

The $LaPO_4$ C (Fig. 2) and C2S (Fig. 3) NPs synthesized using procedure A were characterized with either spherical or ellipsoidal shapes, having a mean particle size of 4.5 ± 1.2 nm and 5.4 ± 0.9 nm, respectively. The lattice fringes from (200) planes of $LaPO_4$ having a hexagonal crystal system were observed in both $LaPO_4$ C and C2S NPs (Figs. 2b and 3b). The resemblance between the mean particle size and the crystallite size suggests that both $LaPO_4$ C and C2S NPs correspond to single crystals. A

similar morphology is expected after varying the concentration of reagents, where <10 nm spherical and ellipsoidal $LaPO_4$ C NPs were obtained after following procedure C (Fig. S3 in the ESI).
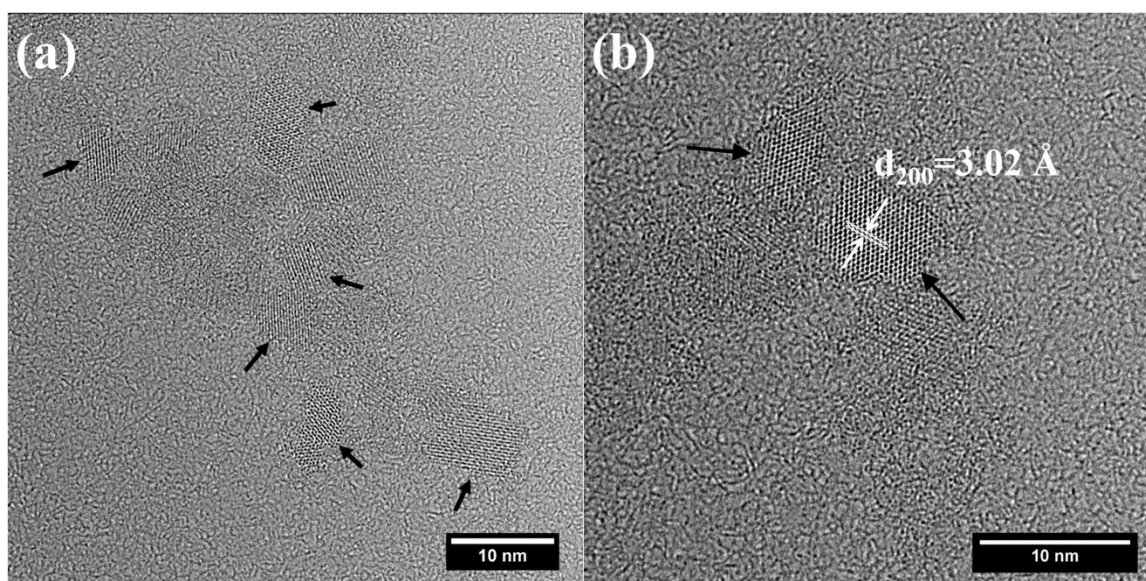
Fig. 2 Spherical and ellipsoidal $LaPO_4$ C NPs synthesized following procedure A. Transmission electron micrographs of $LaPO_4$ C NPs having a mean particle size of 4.5 ± 1.2 nm. $LaPO_4$ C NPs are pointed out by black arrows in (a) and (b), whereas the lattice fringes in a $LaPO_4$ C NP are highlighted in (b). The lattice fringes correspond to the (200) planes having a d_{200} = 3.02 Å.
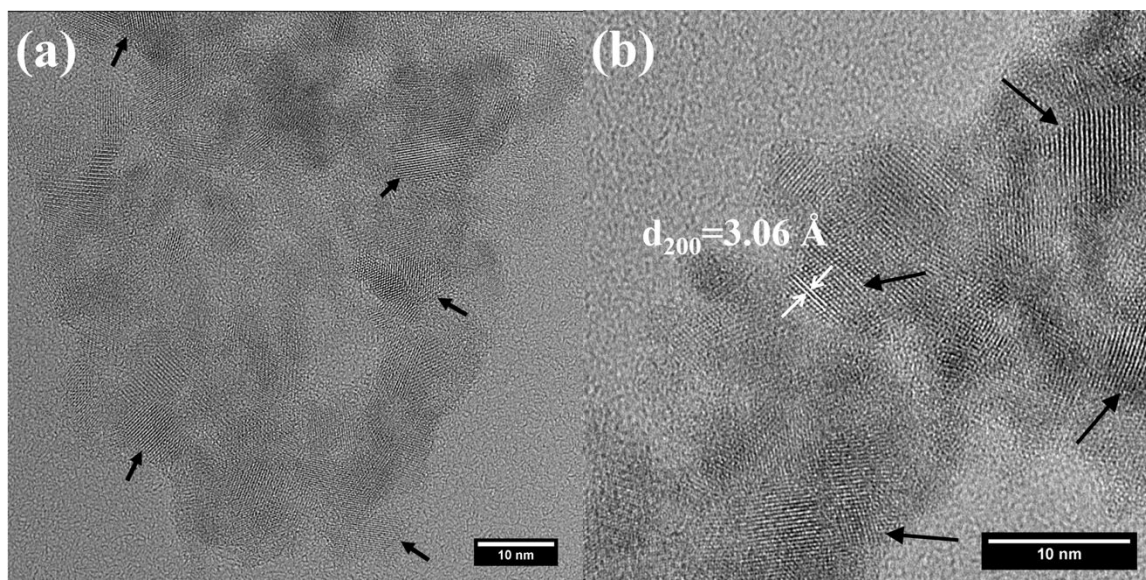
Fig. 3 Spherical and ellipsoidal $LaPO_4$ C2S NPs synthesized following procedure A. Transmission electron micrographs of $LaPO_4$ C2S NPs having a mean particle size of 5.4 ± 0.9 nm. $LaPO_4$ C2S NPs are pointed out by black arrows in (a) and (b), whereas the lattice fringes in a $LaPO_4$ C2S NP are highlighted in (b). The lattice fringes correspond to the (200) planes having a d_{200} = 3.06 Å.

3.3   Size distribution, zeta potential, and stability of LaPO$_4$ C and C2S NPs

Representative size distributions of LaPO$_4$ C and C2S NPs synthesized following different procedures, as described in Table 1, are displayed in Fig. S4 in the ESI. LaPO$_4$ C NPs showed a lower effective diameter compared to that of LaPO$_4$ C2S NPs for the different procedures (Table S2 in the ESI). The small effective diameter (46.6 ± 0.6 nm) and polydispersity index (0.150 ± 0.009) obtained for LaPO$_4$ C NPs synthesized according to procedure B, are associated with an increase in Na$_5$P$_3$O$_{10}$ concentration. The higher concentration of Na$_5$P$_3$O$_{10}$ (1:2 volume ratio of LaCl$_3$:Na$_5$P$_3$O$_{10}$) contributed to a greater fraction of tripolyphosphate (P$_3$O$_{10}^{5-}$) and pyrophosphate (P$_2$O$_7^{4-}$) species that limited the growth and enhanced the stability of the particles. The increase in effective diameter and polydispersity after shell deposition is assumed to be related to aggregation of the particles resulting from consumption of stabilizing species (P$_3$O$_{10}^{5-}$ and P$_2$O$_7^{4-}$). The deposition of nonradioactive LaPO$_4$ shells onto LaPO$_4$ C NPs shifted the zeta potential to less negative values for the different procedures (Table S2 in the ESI). This shift in zeta potential values is associated with the consumption of negatively charged stabilizing species (P$_3$O$_{10}^{5-}$ and P$_2$O$_7^{4-}$) on the particle surface during shell deposition.[60] Overall, a significant difference in the mean zeta potential was observed between LaPO$_4$ C and C2S NPs synthesized by procedures A and C with respect to LaPO$_4$ C and C2S NPs prepared following procedure B ($p < 0.05$).

The fraction of La cations in the dialysate was used as a tool to assess the stability of LaPO$_4$ C NPs, synthesized following procedure A, at different hydrogen ion concentrations (pH 2.4, 3.5, 5.7, 8.8, and 10.0). These hydrogen ion concentrations were selected to study how alkaline and acidic conditions can promote the release of La cations over time and hence influence the stability of LaPO$_4$ NPs. Although LaPO$_4$ C NPs were not exposed to biologically relevant conditions (pH 7.4), the proposed hydrogen ion concentrations encompass a broad range of pH that will help elucidate the response of LaPO$_4$ NPs in the cellular and tumor microenvironment. For instance, the local pH in tumor microenvironments can range between 5.5 and 7.0,[65] whereas a phagolysosomal pH ~4.9 has been measured *in vivo* in alveolar macrophages.[66] The fraction of La in dialysates kept between a pH of 5.7 and 10.0 was <4% (Fig. 4), which is consistent with the 5% of lanthanide ions present on the particle surface shell.[60] As shown in Fig. S5 in the ESI, LaPO$_4$ C NPs dialyzed for 72 h at these conditions (pH 5.7–10.0) yielded multimodal size distributions, having an effective diameter >100 nm and a zeta potential ca. −35 mV (Table S3 in the ESI). Increasing the dialysate pH contributed to an increase in the effective diameter and the polydispersity index of LaPO$_4$ C NPs (Table S3 in the ESI). Decreasing the pH of the dialysate to 3.5 caused a continuous increase in the fraction of La over time to a maximum of 8.0 ± 0.2% after 72 h (Fig. 4). It is assumed that maintaining LaPO$_4$ C NPs at a pH of 3.5 for 72 h may have compromised their stability (i.e., the particles were partially dissolved) because the concentration of La cations in the dialysate was >5%. LaPO$_4$ C NPs dialyzed at a pH of 3.5 were characterized by low colloidal stability associated with a neutral zeta potential (~0 mV), which led to significant particle precipitation during dynamic light scattering characterization. At a pH of 2.4, 103.9 ± 4.4% of La cations were found in the dialysate after 24 h in dialysis, suggesting that LaPO$_4$ C NPs must be kept at a pH greater than 3.5 to prevent their dissolution. Although the likelihood of encountering a pH below 3.5 *in vivo* is only expected within the stomach cavity, LaPO$_4$ NPs showed

great stability over a broad pH range (5.7–10.0). Testing LaPO$_4$ C and C2S NPs over this broad pH range should ensure that the particles are robust enough to survive the *in vivo* tissue and tumor microenvironments.
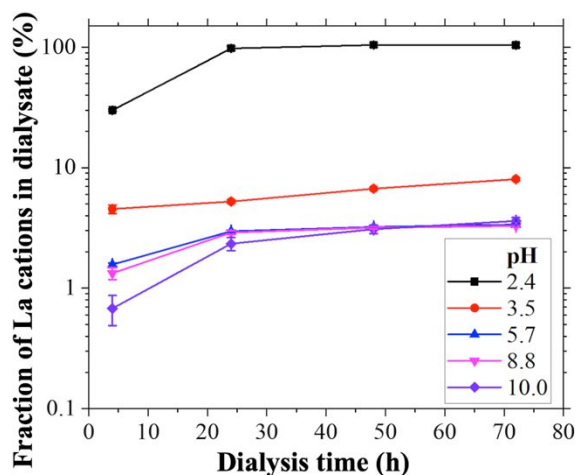
Fig. 4 LaPO$_4$ C NPs are relatively stable above pH 3.5. Fraction of La cations in dialysate over time after dialysis of LaPO$_4$ C NPs, synthesized following procedure A, against deionized water having different hydrogen ion concentrations. Less than 4% of La cations were observed in the dialysate after dialysis at a pH between 5.7 and 10.0, whereas decreasing the pH to 3.5 and 2.4 led to 8.0% and >100% of La cations in the dialysate, respectively.

3.4 Radionuclide encapsulation in La(^{227}Th)PO$_4$ C and C2S NPs

Figure 5 shows the fraction of activity, referred to as *leakage*, in the dialysate of ^{227}Th, ^{223}Ra, and ^{211}Pb from La(^{227}Th)PO$_4$ C and C2S NPs synthesized following procedure A. The leakage of ^{227}Th from La(^{227}Th)PO$_4$ C NPs reached a maximum of 1.0 ± 0.7% after 23 days, while the maximum leakage of decay daughters was 0.8 ± 0.4% for ^{223}Ra and 1.3 ± 0.8% for ^{211}Pb. The deposition of two LaPO$_4$ shells onto La(^{227}Th)PO$_4$ C NPs decreased the activity of radionuclides in the dialysate by one order of magnitude, resulting in a leakage of $\leq 0.08 \pm 0.02$% for ^{227}Th, $\leq 0.13 \pm 0.08$% for ^{223}Ra, and $\leq 0.15 \pm 0.09$% for ^{211}Pb (Fig. 5b). A greater concentration of Na$_5$P$_3$O$_{10}$ during synthesis of La(^{227}Th)PO$_4$ C NPs, samples prepared using procedure B, increased the leakage of radionuclides over time with respect to samples synthesized following procedure A (Fig. 6a). This increase in dialysate activity may be related to the formation of radionuclide complexes, particularly ^{227}Th complexes with pyrophosphate groups (P$_2$O$_7^{4-}$), encouraged by the higher concentration of Na$_5$P$_3$O$_{10}$. The fraction of activity of ^{223}Ra was slightly lower than that of ^{227}Th, whereas the leakage of ^{211}Pb reached a maximum of 10.8 ± 1.0% after 3 days and then decreased to ~4%. The retention of radionuclides was enhanced significantly in La(^{227}Th)PO$_4$ C2S NPs, where all the radionuclides evaluated had a leakage below 0.25%, and in some cases, no activity was found in the dialysate (Fig. 6b). La(^{227}Th)PO$_4$ C NPs, synthesized following procedure C, had a maximum leakage of 0.33 ± 0.05% for ^{227}Th after 6 days, and no activity was detected in the dialysate after 13 days (Fig. 7a). A maximum leakage of 20.3 ± 1.1% for ^{223}Ra and 13.5

± 1.0% for ^{211}Pb was obtained for La(^{227}Th)PO$_4$ C NPs prepared following procedure C. Deposition of two LaPO$_4$ shells enhanced the retention of decay daughters, which showed a continuous increase in activity over time to a maximum of 5.9 ± 0.4% for ^{223}Ra and 6.3 ± 0.5% for ^{211}Pb after 31 days (Fig. 7b). Compared to Gd(^{227}Th)VO$_4$ C and C2S NPs both La(^{227}Th)PO$_4$ C and C2S NPs displayed enhanced encapsulation of ^{227}Th and retention of its decay daughters, ^{223}Ra and ^{211}Pb. The maximum leakage of ^{223}Ra (20.3 ± 1.1%) and ^{211}Pb (13.5 ± 1.0%) obtained in this work were lower than the leakage observed from Gd(^{227}Th)VO$_4$ C2S NPs (~25% for ^{223}Ra and >30% for ^{211}Pb).[44] The enhanced retention of ^{223}Ra and ^{211}Pb within La(^{227}Th)PO$_4$ NPs may be related to the nine-fold coordination of ^{227}Th cations, compared with the eight-fold coordination of ^{227}Th in Gd(^{227}Th)VO$_4$ NPs.[12] It has been calculated based on a La concentration of 0.1 M and the fact that a 5 nm LaPO$_4$ C NP contains ca. 1,000 La cations,[13] that there is roughly 1 ^{227}Th cation per 7,000–29,000 LaPO$_4$ C NPs when using 12–49 µCi of ^{227}Th, respectively. The specific activity of LaPO$_4$ C NPs synthesized by procedure A and C is approximately 4.6 µCi/mg and 46 µCi/mg, respectively. These estimates and the radionuclide encapsulation results suggest that there is ample capacity to increase the specific activity of ^{227}Th in La(^{227}Th)PO$_4$ C NPs for therapeutic applications.
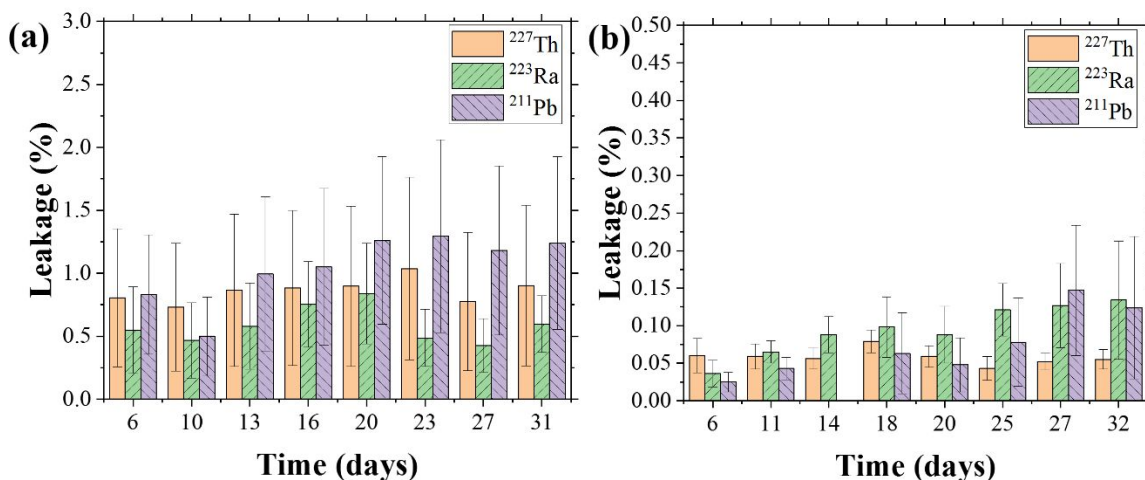
Fig. 5 Enhanced ^{227}Th encapsulation and retention of decay daughters (^{223}Ra and ^{211}Pb) after deposition of two LaPO$_4$ shells onto La(^{227}Th)PO$_4$ NPs synthesized following procedure A. Leakage of ^{227}Th, ^{223}Ra, and ^{211}Pb from La(^{227}Th)PO$_4$ (a) C and (b) C2S NPs. Radionuclide leakage did not exceed 2.0% in La(^{227}Th)PO$_4$ C NPs, whereas a 10-fold reduction in leakage was obtained after deposition of two LaPO$_4$ shells. The results shown are the mean and standard deviation of two and four independent experiments for La(^{227}Th)PO$_4$ C and C2S NPs, respectively.
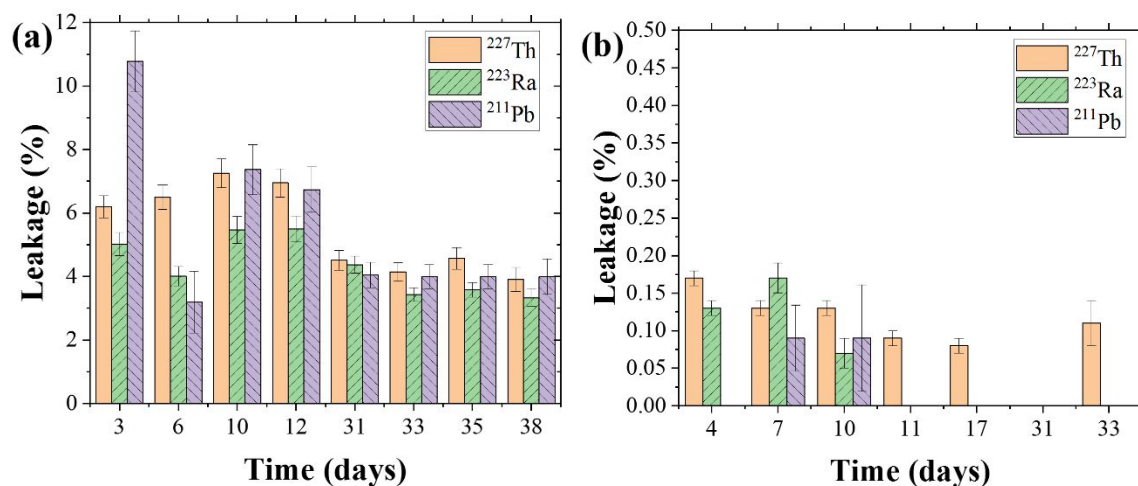
Fig. 6 Enhanced ^{227}Th encapsulation and retention of decay daughters (^{223}Ra and ^{211}Pb) after deposition of two LaPO$_4$ shells onto La(^{227}Th)PO$_4$ NPs synthesized following procedure B. Leakage of ^{227}Th, ^{223}Ra, and ^{211}Pb from La(^{227}Th)PO$_4$ (a) C and (b) C2S NPs. Radionuclide leakage was below 12.0% in La(^{227}Th)PO$_4$ C NPs, whereas less than 0.2% leakage was obtained after deposition of two LaPO$_4$ shells. Data represent the result of a single experiment (see Section 2.4 for propagation of uncertainty details).
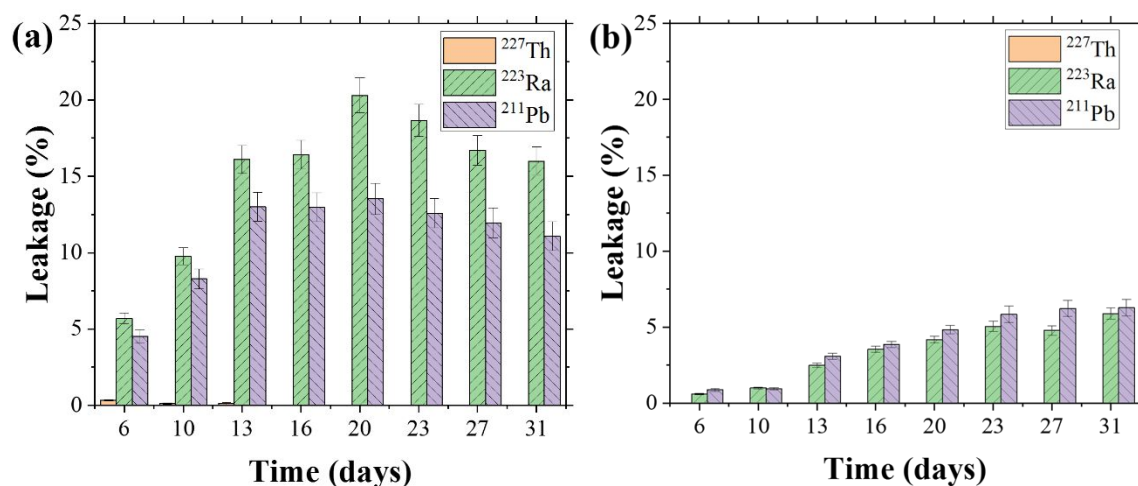
Fig. 7 Enhanced ^{227}Th encapsulation and retention of decay daughters (^{223}Ra and ^{211}Pb) after deposition of two LaPO$_4$ shells onto La(^{227}Th)PO$_4$ NPs synthesized following procedure C. Leakage of ^{227}Th, ^{223}Ra, and ^{211}Pb from La(^{227}Th)PO$_4$ (a) C and (b) C2S NPs. Decay daughter leakage was ~20% in La(^{227}Th)PO$_4$ C NPs, whereas there was a 4-fold decrease in leakage after deposition of two LaPO$_4$ shells. Data represents the result of a single experiment (see Section 2.4 for propagation of uncertainty details).

The ^{227}Th radiochemical yields obtained for La(^{227}Th)PO$_4$ C and C2S NPs prepared by the different procedures are summarized in Table 2. As indicated for procedure A, no significant difference between the radiochemical yields of La(^{227}Th)PO$_4$ C and C2S NPs was observed, and the mean value was >94%. La(^{227}Th)PO$_4$ C NPs prepared following Procedures B and C exhibited ^{227}Th radiochemical yields <90%, while the mean radiochemical yield of La(^{227}Th)PO$_4$ C2S NPs was >92% (Table 2).

Overall, the mean radiochemical yield of La(^{227}Th)PO$_4$ C2S NPs was greater than that of La(^{227}Th)PO$_4$ C NPs for most of the samples. The high ^{227}Th radiochemical yields of La(^{227}Th)PO$_4$ C and C2S NPs may be attributed to the high capacity of the LaPO$_4$ crystal lattice to encapsulate tetravalent actinides.[12] The fraction of ^{227}Th cations adsorbed on the particle surface, due to an electrostatic interaction between Th^{4+} and P$_2$O$_7{}^{4-}$, is likely responsible for the activity of ^{227}Th detected over time in the dialysate for both La(^{227}Th)PO$_4$ C and C2S NPs. For instance, La(^{227}Th)PO$_4$ C NPs prepared following procedure B had a maximum leakage of ^{227}Th of $7.2 \pm 0.4\%$, but less than $1.0 \pm 0.7\%$ of ^{227}Th activity was found in the dialysate when using procedure A. The activity of ^{227}Th in the dialysate decreased after deposition of two LaPO$_4$ shells because the adsorbed surface species were either removed during dialysis, consumed during synthesis, or both.

Table 2 Radiochemical yields of La(^{227}Th)PO$_4$ C and C2S NPs synthesized using different procedures.

	Radiochemical yield (%)	
Procedure	La(^{227}Th)PO$_4$ C	La(^{227}Th)PO$_4$ C2S
A	96.8 ± 2.3	94.4 ± 3.8
B	87.5 ± 11.4	92.4 ± 11.7
C	85.8 ± 11.5	98.1 ± 12.6

The lower leakage of ^{223}Ra compared with that of ^{227}Th from La(^{227}Th)PO$_4$ C NPs, synthesized using procedures A and B (Figs. 5 and 6), is attributed to ^{223}Ra leaking from the particles while the fraction of ^{227}Th in the dialysate originates from cations adsorbed onto the particle surface. The higher activity of ^{211}Pb in the dialysate relative to both ^{227}Th and ^{223}Ra is associated with its greater recoil energy compared to ^{223}Ra, and the fact that ^{211}Pb is the fourth decay daughter. The partial retention of ^{223}Ra and ^{211}Pb in La(^{227}Th)PO$_4$ C and C2S NPs is attributed to their recoil energy and hence, their range within LaPO$_4$.[13] In LaPO$_4$ with an estimated density of 5.12 g/cm^3 the range of ^{223}Ra (~110 keV) and ^{211}Pb (~140 keV) is 27.0 nm and 32.6 nm, respectively.[67] Recoil energies were calculated using classical conservation of momentum, whereas the Stopping and Range of Ions in Matter program was used to estimate the range of radionuclides in LaPO$_4$. Based on the calculated recoil energies and ranges, a greater fraction of ^{223}Ra and ^{211}Pb activity would normally be detected in the dialysate (~100%), for both La(^{227}Th)PO$_4$ C and C2S NPs, than was observed. Potentially, the recoil energy of each decay daughter is partially distributed to the NP by translational, rotational, and vibrational modes.[13,68,69] Considering the complex bond structure of a NP and its relative mass with respect to that of the decay daughter, the effective recoil energy available for bond rupture may be decreased by ~10^3.[13,68] A simplified mathematical expression for the effective energy available for bond breaking is represented by

$$E_r^{eff} = E_r^{max}\frac{M_{DD}}{M_{DD} + M_{NP}},$$

where E_r^{max} is the maximum recoil energy, M_{DD} is the atomic weight of the decay daughter, and M_{NP} is the molecular weight of the NP.[13,68] Therefore, a low effective energy for bond rupture will result in a shorter range of decay daughters in $LaPO_4$ and hence, greater retention. The leakage of ^{223}Ra and ^{211}Pb decreased after the deposition of two $LaPO_4$ shells onto $La(^{227}Th)PO_4$ C NPs for each of the different synthesis procedures (Figs. 5–7). This enhanced radioisotope retention is partially attributed to the nonradioactive shells functioning as a dense atomic barrier,[14,16,43,44] which prevents decay daughters from leaking. The greater mass and moment of inertia of the $La(^{227}Th)PO_4$ C2S relative to that of the $La(^{227}Th)PO_4$ C NPs may also lead to a larger fraction of the recoil energy being distributed through translational and rotational modes, which in turn enhances the retention of decay daughters.

3.5   Cytotoxicity of LaPO₄ C and C2S NPs

$LaPO_4$ C and C2S NP suspensions prepared using procedure A were selected for cytotoxic evaluation given the high radionuclide encapsulation obtained with $La(^{227}Th)PO_4$ C and C2S NPs and hence their promising application in TAT. The cytotoxicity of $LaPO_4$ C and C2S NPs was assessed by measuring the metabolic activity (MTT assay) of RAW 264.7 murine macrophage and BT-474 human breast cancer cells cultured in monolayer formats. The cell viability of RAW 264.7 cells was ~90% for concentrations of $LaPO_4$ C NPs between 29.2 µg/mL and 58.5 µg/mL, >100% from 116.9 µg/mL to 935.5 µg/mL, and <60% for 1,817 µg/mL (Fig. 8). A decrease to ~90% in cell viability between 29.2 µg/mL and 58.5 µg/mL may be attributed to a shift in zeta potential values to less negative (Table S4 in the ESI), which may facilitate an electrostatic interaction between the particles and the cell membrane.[70] The shift in zeta potential to less negative values as a consequence of NP concentration is related to contributions from extraneous particulate matter and has also been associated with an increase in particle size.[71] Compared with $LaPO_4$ C NPs, $LaPO_4$ C2S NPs displayed higher cytotoxicity for all the concentrations evaluated (Fig. 8), and at 935.5 µg/mL and 1,817 µg/mL, the cell viability dropped to 55.1 ± 1.4% and 16.8 ± 1.2%, respectively. The greater toxicity exhibited by $LaPO_4$ C2S NPs on RAW 264.7 cells is assumed to be related to their larger size compared with that of $LaPO_4$ C NPs. Overall, no significant morphological changes in RAW 264.7 macrophage cells were observed after incubation for 24 h with $LaPO_4$ C and C2S NPs and an increase in cell density shows that the NPs did not significantly alter the cell growth (Fig. S6 in the ESI).
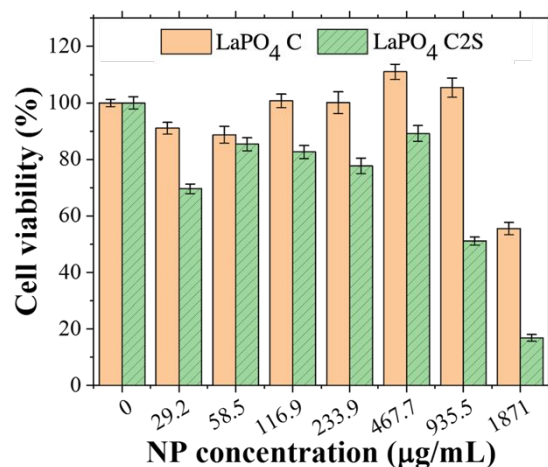
Fig. 8 LaPO$_4$ C2S NPs are more cytotoxic to murine macrophage cells than LaPO$_4$ C NPs. The cell viability of RAW 264.7 murine macrophage cell line was determined by MTT assay after exposure for 24 h to different concentrations of LaPO$_4$ C and C2S NPs prepared following procedure A.

Neither LaPO$_4$ C nor C2S NPs exhibited toxic effects to monolayers of BT-474 cells at concentrations ranging from 29.2 µg/mL to 233.9 µg/mL (Fig. 9a), suggesting that BT-474 cells may be less sensitive than RAW 264.7 cells to the changes in concentration, size, and zeta potential of both LaPO$_4$ C and C2S NPs. Increasing the concentration of LaPO$_4$ C NPs above 467.7 µg/mL led to a decrease in cell viability below 51.9 ± 8.0%, whereas the cell viability was ~30% for concentrations of LaPO$_4$ C2S NPs exceeding 935.5 µg/mL. At the highest concentration (1,871 µg/mL), a significant precipitation of particles was observed which led to RAW 264.7 and BT-474 cells being completely coated with the NPs, potentially limiting their access to nutrients and thereby inducing a greater cytotoxic effect. Morphological changes in BT-474 cells after incubation with either LaPO$_4$ C or C2S NPs were difficult to assess due to the significant precipitation of particles on top of the cells even at the lowest concentration (Fig. S7 in the ESI). Assessment of particle cytotoxicity using BT-474 spheroids takes advantage of a heterogeneous model where cell–cell interactions, oxygen gradients, and particle exposure provide a better approximation of *in vivo* tissue microenvironments.[72–74] BT-474 spheroids with an average diameter of 441.2 ± 17.5 µm were obtained after incubation of 3×10^3 cells per well for 72 h (Fig. S8 in the ESI). A decrease in cell viability with increasing concentration of both LaPO$_4$ C and C2S NPs was observed with BT-474 spheroids (Fig. 9b). Both LaPO$_4$ C and C2S NPs exerted cytotoxic effects on BT-474 cells when the concentration was >58.5 µg/mL, as evidenced by a cell viability <50%. The toxicity exerted by LaPO$_4$ C2S NPs on BT-474 was significantly higher relative to that observed for all concentrations of LaPO$_4$ C NPs (p < 0.01). The U-shape of the plate allowed for precipitation of NPs beneath and around BT-474 cell spheroids, increasing the overall relative exposure of cells to LaPO$_4$ C and C2S NPs (Fig. S8 in the ESI). Further investigation is required to assess the cellular uptake, cytotoxic effects, and localization of LaPO$_4$ C and C2S NPs in both monolayer and spheroid cultures. Surface modification of LaPO$_4$ NPs to attach fluorescent dyes will allow for tracking of the cellular localization and identification of the potential associated cytotoxic effects. A feasible approach to label LaPO$_4$ NPs with fluorescent dyes as well as targeting vectors may be based on carbodiimide crosslinker chemistry.[13] These experiments will serve as controls when testing

and understanding the therapeutic effect (i.e., cytotoxicity) of La(^{227}Th)PO$_4$ C and C2S NPs in both monolayer and spheroid cultures.
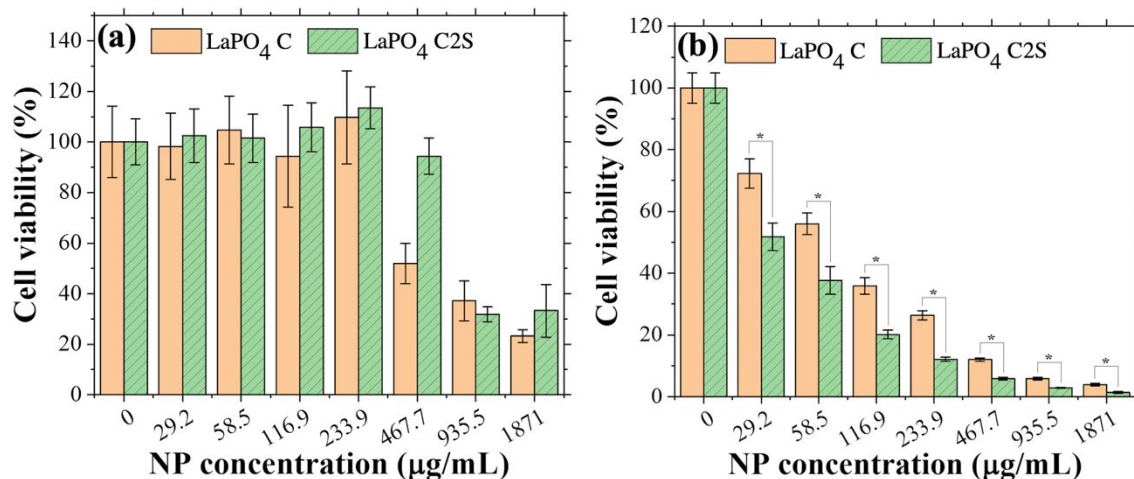
Figure 9 Greater cytotoxic effect of LaPO$_4$ C and C2S NPs on BT-474 human breast cancer cell spheroids relative to monolayer cultures. The cell viability of BT-474 cells in (a) monolayer culture and (b) spheroids was determined by MTT and CellTiter-Glo® 3D assays, respectively, after exposure for 24 h to different concentrations of LaPO$_4$ C and C2S NPs prepared following procedure A. * denotes statistically significant difference when compared cell viability of LaPO$_4$ C and C2S NPs at each concentration (p < 0.01).

4   Conclusions

La(^{227}Th)PO$_4$ C and C2S NPs were evaluated as radionuclide delivery platforms for TAT applications to leverage their potential to encapsulate ^{227}Th and retain decay daughters at the treatment site. This has the two-fold advantage of minimizing potential damage to normal tissue from circulating decay daughters (^{223}Ra and ^{211}Pb), while also increasing the local impact at the tumor site. The morphology, surface charge, and cytotoxicity of LaPO$_4$ C and C2S NPs without their ^{227}Th payload were characterized. Morphological characterization of LaPO$_4$ C and C2S NPs showed particles having a mean particle size below 6 nm with spherical and ellipsoidal shape, where the mean particle size and the crystallite size increased after the deposition of two LaPO$_4$ shells onto LaPO$_4$ C NPs. High encapsulation of ^{227}Th was evidenced by the low levels of activity detected in the dialysate with a maximum leakage of 7.2 ± 0.4% and 0.17 ± 0.01% from La(^{227}Th)PO$_4$ C and C2S NPs, respectively. Deposition of two nonradioactive LaPO$_4$ shells contributed to a significant increase in decay daughter retention (>93.7%) with respect to that obtained for La(^{227}Th)PO$_4$ C NPs (<80%). The cytotoxic effects of nonradioactive LaPO$_4$ C and C2S NPs were evaluated in both cancer (epithelial) and immune (macrophage) cells types. Initial evaluation using monolayer configurations indicated that both LaPO$_4$ C and C2S NPs induced a significant decrease in cell viability at high concentrations (>935.5 μg/mL) for both BT-474 and RAW 264.7 cells. By comparison, BT-474 spheroids exposed to LaPO$_4$ C and C2S NPs were more sensitive than BT-474 monolayer cultures. These results may point to a potentially additive effect of LaPO$_4$ C and C2S NPs that could be leveraged for treating solid micrometastatic

tumors. Current efforts are focused on the surface modification of LaPO$_4$ NPs with fluorescent dyes to assess their toxic effect based on cellular interactions and allow visual localization within individual cells and within tumor spheroids.

Conflicts of interest

There are no conflicts to declare.

Acknowledgements

References

1 A. Thust, A. Hirsch, E. Haussühl, N. Schrodt, L. Loison, P. Schott, L. Peters, G. Roth and B. Winkler, *Phys Chem Minerals*, 2018, **45**, 323–332.
2 M. R. Rafiuddin and A. P. Grosvenor, *Journal of Alloys and Compounds*, 2015, **653**, 279–289.
3 N. Dacheux, N. Clavier and R. Podor, *American Mineralogist*, 2013, **98**, 833–847.
4 J. S. Luo and G. K. Liu, *Journal of Materials Research*, 2001, **16**, 366–372.
5 A. Meldrum, L. A. Boatner and A. R. C. Ewing, *Mineralogical Magazine*, 2000, **64**, 185–194.
6 a E. Grechanovsky, N. N. Eremin and V. S. Urusov, *Lattice Dynamics*, 2013, **55**, 1929–1935.
7 Y. Ji, P. M. Kowalski, S. Neumeier, G. Deissmann, P. K. Kulriya and J. D. Gale, *Nuclear Instruments and Methods in Physics Research B*, 2017, **393**, 54–58.
8 P. M. Kowalski, Y. Ji, Y. Li, Y. Arinicheva, G. Beridze, S. Neumeier, A. Bukaemskiy and D. Bosbach, *Nuclear Inst. and Methods in Physics Research, B*, 2017, **393**, 68–72.
9 V. S. Urusov, A. E. Grechanovsky and N. N. Eremin, *Glass Physics and Chemistry*, 2012, **38**, 55–62.
10 a. Meldrum, L. Boatner and R. Ewing, *Physical Review B*, 1997, **56**, 13805–13814.
11 A. Meldrum, L. A. Boatner, W. J. Weber and R. C. Ewing, *Geochimica et Cosmochimica Acta*, 1998, **62**, 2509–2520.
12 S. Neumeier, Y. Arinicheva, Y. Ji, J. M. Heuser, P. M. Kowalski, P. Kegler, H. Schlenz, D. Bosbach and G. Deissmann, *Radiochim. Acta*, 2017, **105**, 961–984.
13 J. Woodward, S. J. Kennel, A. Stuckey, D. Osborne, J. Wall, A. J. Rondinone, R. F. Standaert and S. Mirzadeh, *Bioconjugate Chemistry*, 2011, **22**, 766–776.
14 B. M. F. McLaughlin, J. Woodward, R. A. Boll, A. J. Rondinone, S. Mirzadeh and J. D. Robertson, *Radiochim*, 2013, **101**, 595–600.
15 M. F. McLaughlin, J. Woodward, R. A. Boll, J. S. Wall, A. J. Rondinone, S. J. Kennel, S. Mirzadeh and J. D. Robertson, *PLoS ONE*, 2013, **8**, 2–9.
16 J. V. Rojas, J. D. Woodward, N. Chen, A. J. Rondinone, C. H. Castano and S. Mirzadeh, *Nuclear Medicine and Biology*, 2015, **42**, 614–620.

17 W. Ren, G. Tian, L. Zhou, W. Yin, L. Yan, S. Jin, Y. Zu, S. Li, Z. Gu and Y. Zhao, *Nanoscale*, 2012, **4**, 3754.

18 S. Rodriguez-Liviano, A. I. Becerro, D. Alcántara, V. Grazú, J. M. De La Fuente and M. Ocaña, *Inorganic Chemistry*, 2013, **52**, 647–654.

19 M. Toro-Gonzalez, D. M. Clifford, R. Copping, S. Mirzadeh and J. V. Rojas, *Journal of Nanoparticle Research*, 2018, **20**, 238.

20 N. Sobol, L. Sutherlin, E. Cedrowska, J. Schorp, C. Rodríguez-Rodríguez, J. Lattimer, D. C. Miller, P. Pevsner and J. D. Robertson, *APL Bioengineering*, 2018, **2**, 016101.

21 Y. Li, T. Chen, W. Tan and D. R. Talham, *Langmuir*, 2014, **30**, 5873–5879.

22 C. Parker, V. Lewington, N. Shore, C. Kratochwil, M. Levy, O. Lindén, W. Noordzij, J. Park and F. Saad, *JAMA Oncol*, 2018, **4**, 1765–1772.

23 R. H. Larsen, J. Borrebaek, J. Dahle, K. B. Melhus, C. Krogh, M. H. Valan and Ø. S. Bruland, *Cancer Biotherapy and Radiopharmaceuticals*, 2007, **22**, 431–437.

24 U. B. Hagemann, D. Mihaylova, S. R. Uran, J. Borrebaek, D. Grant, R. M. Bjerke, J. Karlsson and A. S. Cuthbertson, *Oncotarget*, 2017, **8**, 56311–56326.

25 J. Dahle, C. Krogh, K. B. Melhus, J. Borrebæk, R. H. Larsen and Y. Kvinnsland, *International Journal of Radiation Oncology Biology Physics*, 2009, **75**, 886–895.

26 U. B. Hagemann, K. Wickstroem, E. Wang, A. O. Shea, K. Sponheim, J. Karlsson, R. M. Bjerke, O. B. Ryan and A. S. Cuthbertson, *Molecular Cancer Therapeutics*, 2016, **15**, 2422–2431.

27 T. Ramdahl, H. T. Bonge-Hansen, O. B. Ryan, Å. Larsen, G. Herstad, M. Sandberg, R. M. Bjerke, D. Grant, E. M. Brevik and A. S. Cuthbertson, *Bioorganic and Medicinal Chemistry Letters*, 2016, **26**, 4318–4321.

28 J. Dahle and R. Larsen, *Current Radiopharmaceuticalse*, 2008, **1**, 209–214.

29 J. Dahle, J. Borrebaek, T. J. Jonasdottir, A. K. Hjelmerud, K. B. Melhus, Ø. S. Bruland, O. W. Press and R. H. Larsen, *Blood*, 2007, **110**, 2049–2056.

30 J. Dahle, J. Borrebæk, K. B. Melhus, Ø. S. Bruland, G. Salberg, D. R. Olsen and R. H. Larsen, *Nuclear Medicine and Biology*, 2006, **33**, 271–279.

31 N. Abbas, H. Heyerdahl, Ø. S. Bruland, J. Borrebæk, J. Nesland and J. Dahle, *EJNMMI Research*, 2011, **1**, 1–12.

32 U. B. Hagemann, C. Ellingsen, J. Schuhmacher, A. Kristian, A. Mobergslien, V. Cruciani, K. Wickstroem, C. A. Schatz, C. Kneip, S. Golfier, R. Smeets, S. Uran, H. Hennekes, J. Karlsson, R. M. Bjerke, O. B. Ryan, D. Mumberg, K. Ziegelbauer and A. S. Cuthbertson, *Clin. Cancer Res.*, 2019, **25**, 4723–4734.

33 L. Thijssen, D. R. Schaart, D. de Vries, A. Morgenstern, F. Bruchertseifer and A. G. Denkova, *Radiochimica Acta*, 2012, **100**, 473–482.

34 R. M. De Kruijff, K. Drost, L. Thijssen, A. Morgenstern, F. Bruchertseifer, D. Lathouwers, H. T. Wolterbeek and A. G. Denkova, *Applied Radiation and Isotopes*, 2017, **128**, 183–189.

35 R. M. de Kruijff, A. J. G. M. van der Meer, C. A. A. Windmeijer, J. J. M. Kouwenberg, A. Morgenstern, F. Bruchertseifer, P. Sminia and A. G. Denkova, *European Journal of Pharmaceutics and Biopharmaceutics*, 2018, **127**, 85–91.

36 G. Wang, R. M. De Kruijff, A. Rol, L. Thijssen, E. Mendes, A. Morgenstern, F. Bruchertseifer, M. C. A. Stuart, H. T. Wolterbeek and A. G. Denkova, *Applied Radiation and Isotopes*, 2014, **85**, 45–53.

37 M. Y. Change, J. Seideman and S. Sofou, *Bioconjugate Chemistry*, 2008, **19**, 1274–1282.

38 S. Sofou, B. J. Kappel, J. S. Jaggi, M. R. Mcdevitt, D. A. Scheinberg and G. Sgouros, *Bioconjugate Chemistry*, 2007, **18**, 2061–2067.

39 S. Sofou, J. L. Thomas, H. Lin, M. R. McDevitt, D. A. Scheinberg and G. Sgouros, *Journal of Nuclear Medicine*, 2004, **45**, 253–260.

40 G. Henriksen, B. W. Schoultz, T. E. Michaelsen, S. Bruland and R. H. Larsen, *Nuclear Medicine and Biology*, 2004, **31**, 441–449.

41 T. J. Jonasdottir, D. R. Fisher, J. Borrebæk, Ø. S. Bruland and R. H. Larsen, *Anticancer Research*, 2006, **26**, 2841–2848.

42 R. M. de de Kruijff, R. Raavé, A. Kip, J. Molkenboer-Kuenen, A. Morgenstern, F. Bruchertseifer, S. Heskamp and A. G. Denkova, *Sci Rep*, 2019, **9**, 1–13.

43 M. Toro-González, R. Copping, S. Mirzadeh and J. V. Rojas, *Journal of Materials Chemistry B*, 2018, **6**, 7985–7997.

44 M. Toro-González, A. N. Dame, S. Mirzadeh and J. V. Rojas, *Journal of Applied Physics*, 2019, **125**, 214901.

45 A. Piotrowska, E. Leszczuk, F. Bruchertseifer, A. Morgenstern and A. Bilewicz, *Journal of Nanoparticle Research*, 2013, **15**, 1–11.

46 A. Piotrowska, S. Męczyńska-Wielgosz, A. Majkowska-Pilip, P. Koźmiński, G. Wójciuk, E. Cędrowska, F. Bruchertseifer, A. Morgenstern, M. Kruszewski and A. Bilewicz, *Nuclear Medicine and Biology*, 2017, **47**, 10–18.

47 O. Mokhodoeva, M. Vlk, E. Málková, E. Kukleva, P. Mičolová, K. Štamberg, M. Šlouf, R. Dzhenloda and J. Kozempel, *Journal of Nanoparticle Research*, 2016, **18**, 301.

48 E. Cędrowska, M. Pruszyński, W. Gawęda, M. Żuk, P. Krysiński, F. Bruchertseifer, A. Morgenstern, M.-A. Karageorgou, P. Bouziotis and A. Bilewicz, *Molecules*, 2020, **25**, 1025.

49 A. N. Vasiliev, A. Severin, E. Lapshina, E. Chernykh, S. Ermolaev and S. Kalmykov, *Journal of Radioanalytical and Nuclear Chemistry*, 2017, **311**, 1503–1509.

50 J. Kozempel, M. Vlk, E. Málková, A. Bajzíková, J. Bárta, R. Santos-Oliveira and A. Malta Rossi, *Journal of Radioanalytical and Nuclear Chemistry*, 2015, **304**, 443–447.

51 A. V. Severin, A. N. Vasiliev, A. V. Gopin, I. E. Vlasova and E. V. Chernykh, *Radiochemistry*, 2019, **61**, 339–346.

52 E.-A. Salvanou, D. Stellas, C. Tsoukalas, B. Mavroidi, M. Paravatou-Petsotas, N. Kalogeropoulos, S. Xanthopoulos, F. Denat, G. Laurent, R. Bazzi, S. Roux and P. Bouziotis, *Pharmaceutics*, 2020, **12**, 188.

53 S. Westrøm, M. Malenge, I. S. Jorstad, E. Napoli, Ø. S. Bruland, T. B. Bønsdorff and R. H. Larsen, *Journal of Labelled Compounds and Radiopharmaceuticals*, 2018, **61**, 472–486.

54 S. Westrøm, T. B. Bønsdorff, Ø. S. Bruland and R. H. Larsen, *Translational Oncology*, 2018, **11**, 259–267.

55 F. Reissig, R. Hübner, J. Steinbach, H.-J. Pietzsch and C. Mamat, *Inorg. Chem. Front.*, 2019, **6**, 1341–1349.

56 E. Cędrowska, M. Pruszynski, A. Majkowska-Pilip, S. Męczyńska-Wielgosz, F. Bruchertseifer, A. Morgenstern and A. Bilewicz, *J Nanopart Res*, 2018, **20**, 83.

57 M. Gott, P. Yang, U. Kortz, H. Stephan, H.-J. Pietzsch and C. Mamat, *Chem. Commun.*, 2019, **55**, 7631–7634.

58 L. Kong, W. Smith and D. Hao, *J Cell Mol Med*, 2019, **23**, 3077–3087.

59 V. Buissette, M. Moreau, T. Gacoin and J.-P. Boilot, *Advanced Functional Materials*, 2006, **16**, 351–355.

60 V. Buissette, M. Moreau, T. Gacoin, J. P. Boilot, J. Y. Chane-Ching and T. Le Mercier, *Chemistry of Materials*, 2004, **16**, 3767–3773.

61 Nudat 2, https://www.nndc.bnl.gov/nudat2/index.jsp, (accessed November 16, 2019).

62 M. Runowski, K. Dąbrowska, T. Grzyb, P. Miernikiewicz and S. Lis, *J Nanopart Res*, 2013, **15**, 2068.
63 T. Mosmann, *J. Immunol. Methods*, 1983, **65**, 55–63.
64 Promega, CellTiter-Glo® 3D Cell Viability Assay Protocol, https://www.promega.com/resources/protocols/technical-manuals/101/celltiter-glo-3d-cell-viability-assay-protocol/, (accessed September 19, 2019).
65 C. R. Justus, L. Dong and L. V. Yang, *Front Physiol*, 2013, **4**, 354.
66 K. Nyberg, U. Johansson, A. Johansson and P. Camner, *Environ Health Perspect*, 1992, **97**, 149–152.
67 J. F. Ziegler, M. D. Ziegler and J. P. Biersack, *SRIM-The Stopping and Range of Ions in Matter (2010)*, 2010.
68 S. Mirzadeh, K. Kumar and O. A. Gansow, *Radiochimica Acta*, 1993, **60**, 1–10.
69 C. Hsiung and A. A. Gordus, *The Journal of Chemical Physics*, 1962, **36**, 947–953.
70 Y.-I. Chung, J. C. Kim, Y. H. Kim, G. Tae, S.-Y. Lee, K. Kim and I. C. Kwon, *Journal of Controlled Release*, 2010, **143**, 374–382.
71 R. Tantra, P. Schulze and P. Quincey, *Particuology*, 2010, **8**, 279–285.
72 J. Lee, G. D. Lilly, R. C. Doty, P. Podsiadlo and N. A. Kotov, *Small*, 2009, **5**, 1213–1221.
73 A. Theumer, C. Gräfe, F. Bähring, C. Bergemann, A. Hochhaus and J. H. Clement, *Journal of Magnetism and Magnetic Materials*, 2015, **380**, 27–33.
74 F. Sambale, A. Lavrentieva, F. Stahl, C. Blume, M. Stiesch, C. Kasper, D. Bahnemann and T. Scheper, *J. Biotechnol.*, 2015, **205**, 120–129.

TABLE OF CONTENTS
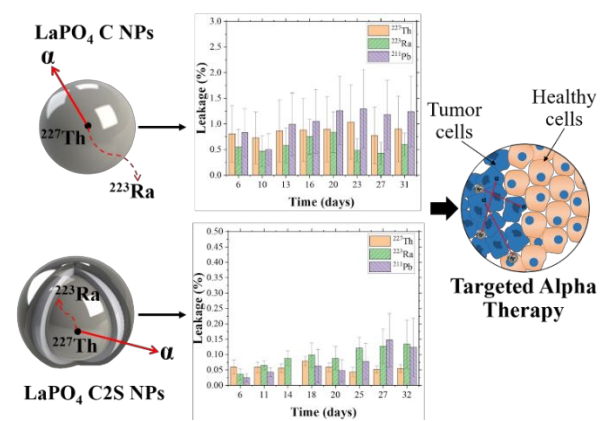
La(^{227}Th)PO$_4$ core +2 shells nanoparticles retained >99.75% of activity from ^{227}Th and decay daughters (^{223}Ra, ^{211}Pb) for targeted alpha therapy.